ARTICLE

Tribological Properties of Poly(L-lysine)-*graft*-poly(ethylene glycol) Films: Influence of Polymer Architecture and Adsorbed Conformation

Scott S. Perry,*,† Xiaoping Yan,‡ F. T. Limpoco,§ Seunghwan Lee,|| Markus Müller,|| and Nicholas D. Spencer||

Departments of Materials Science & Engineering and of Chemistry, University of Florida, Gainesville, Florida 32611, Seagate Technology, 1251 Waterfront Place, Pittsburgh, Pennsylvania 15222, and Laboratory for Surface Science and Technology, Department of Materials, Swiss Federal Institute of Technology, ETH-Hönggerberg, Wolfgang-Pauli-Strasse 10, CH-8093 Zürich, Switzerland

ABSTRACT The tribological properties of poly(L-lysine)-*graft*-poly(ethylene glycol) (PLL-*g*-PEG)-coated oxide interfaces have been investigated with atomic force microscopy (AFM) as a function of the molecular structure. Polymer-bearing surfaces were obtained via spontaneous adsorption of the polymer onto the oxide substrate from a buffered solution of physiological pH. Interfacial friction of these PLL-*g*-PEG-coated surfaces was found to be highly dependent on the duration of deposition and the architecture of PLL-*g*-PEG. In terms of the architecture, the PEG *chain length* and the *grafting ratio* (i.e., the molar ratio of L-lysine monomer to PEG side chain) of adsorbed PLL-*g*-PEG significantly influence the interfacial friction; specifically, friction is reduced as the PEG chain length increases and as the molar ratio of L-lysine monomer to PEG side chain decreases. The characteristics of the polymer deposition time and the influence of the lysine/PEG grafting ratio are rationalized in terms of spatial packing density considerations.

KEYWORDS: atomic force microscopy • friction • lubrication • thin films • polymer coatings • poly(L-lysine)-*graft*-poly(ethylene glycol) • polymer architecture • grafting ratio • silicon oxide

1. INTRODUCTION

Poly(L-lysine)-*graft*-poly(ethylene glycol) (PLL-*g*-PEG) is a member of a family of polycationic PEG-grafted copolymers that have been shown to adsorb on negatively charged surfaces, including various metal oxides, providing a high degree of resistance to protein adsorption (1−3). As a result, PLL-*g*-PEG-modified surfaces have received strong interest in a variety of applications including sensor chips for bioaffinity assays and blood-contacting biomedical devices (4, 5). Similarly, making use of its spontaneous adsorption onto metal oxide surfaces, PLL-*g*-PEG is expected to significantly lubricate these interfaces in physiological aqueous environments by forming a boundary polymer brush layer. As with protein resistance, the lubrication of metal oxide surfaces is of great significance in medical applications.

The structure of PLL-*g*-PEG, depicted in Figure 1, consists of a PLL backbone with multiple PEG side chains that have been grafted onto the backbone via amino groups on a fraction of the lysine units. The remaining amino groups provide the pathway for electrostatic interaction of the PLL backbone with appropriately charged surfaces (1).

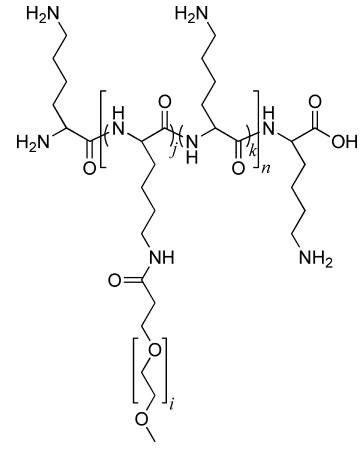

FIGURE 1. Schematic structure of a PLL-*g*-PEG copolymer consisting of a PLL backbone and randomly grafted PEG side chains. In this scheme, $(k + j)/j$ represents the *grafting ratio*, the fraction of lysine units to PEG side chains, for very large n.

In earlier nanotribological investigations using atomic force microscopy (AFM) (6, 7), a significant reduction in the interfacial friction measured between silicon oxide substrates and a sodium borosilicate microsphere was observed upon adsorption of PLL-*g*-PEG on either one or both sides of the interface. In addition, an investigation of PLL-*g*-PEG polymers, differing only in the PEG side-chain length, revealed that interfacial forces measured under aqueous con-

* Author to whom correspondence should be addressed.
Received for review February 16, 2009 and accepted May 5, 2009
† Department of Materials Science & Engineering, University of Florida.
‡ Seagate Technology.
§ Department of Chemistry, University of Florida.
|| Swiss Federal Institute of Technology.
DOI: 10.1021/am900101m

Published on Web 05/22/2009

ditions were reduced with increasing PEG chain length, indicating that interfacial adhesion and friction can be modified through control of the polymer molecular structure (7). Macroscopic investigations showed that the boundary-lubrication properties of aqueous buffer solutions were significantly improved upon addition of PLL-*g*-PEG, with, again, a strong polymer architecture dependence (8, 9).

In this report, we present a systematic investigation of the dependence of interfacial friction on the molecular architecture of PLL-*g*-PEG brush polymers adsorbed on oxide surfaces. In brush systems, the grafting ratio of backbone to side-chain entities represents one of the most significant synthetic design opportunities. While the influence of the grafting ratio on the solution properties is well understood, less is known regarding how this parameter influences interfacial properties such as adsorption and interfacial friction. To this end, we have employed AFM, a quartz crystal microbalance (QCM), and optical waveguide lightmode spectroscopy (OWLS) to methodically explore a matrix of polymer brushes in which the grafting ratio is systematically varied for a series of side-chain molecular weights. In these studies, we have used a sodium borosilicate microsphere, attached to the end of an AFM cantilever, as the probe to avoid substantial deformation of the polymer layer that would occur under the high contact pressures common in the use of conventional (<100 nm radius) Si_3N_4 tips. Interfacial friction measurements were carried out in a *N*-(2-hydroxyethyl)piperazine-*N*'-2-ethanesulfonic acid (HEPES) buffer solution on polymer-coated silicon oxide substrates with bare microsphere probes. Results for three series of polymer samples, distinguished by the PEG molecular weight, are reported; within each series, the polymers differed only in the lysine/PEG ratio (i.e., the *grafting ratio* or the molar ratio of L-lysine-mers to PEG side chains). On the basis of friction measurements on a series of silicon oxide substrates coated with PLL-*g*-PEG that varied only in their grafting ratios, it was observed that the lysine/PEG fraction substantially influences the interfacial friction of these polymer-associated interfaces in a manner intimately tied to the conformation of PEG side chains extending into the solution. These results have been rationalized in terms of the PEG packing density on the surface using scaling arguments.

2. EXPERIMENTAL SECTION

2.1. Synthesis of PLL-*g*-PEG. In this paper, polymer substrates are designated as PLL(*x*)-*g*[*y*]-PEG(*z*), where the copolymer consists of a PLL backbone of molecular weight *x* kDa and a grafted PEG side chain of molecular weight *z* kDa with a grafting ratio [(lysine-mers)/(PEG side chains)] of *y*.

The PLL-*g*-PEG copolymers were synthesized according to a previously described method (1, 2). Briefly, poly(L-lysine) hydrobromide (PLL-HBr, MW 20 kDa; Sigma, St. Louis, MO) was dissolved in a 50 mM sodium borate buffer solution, followed by filter sterilization of the solution (0.22 μm pore-size filter). The *N*-hydroxysuccinimidyl ester of methoxypoly(ethylene glycol)propionic acid (SPA-PEG; Shearwater Polymers, Inc., Huntsville, AL) was then added to the dissolved PLL-HBr. The reaction was allowed to proceed for 6 h at room temperature, after which the reaction mixture was dialyzed (SpectraPor, MW cutoff size 6−8 kDa, Spectrum, Houston, TX) against deionized water for 48 h. The product was freeze-dried and stored at −20 °C.

Through variation of the molecular weight and the amount of starting material (PLL-HBr and SPA-PEG) as well as effective control of the reaction progress, a series of PLL-*g*-PEG graft copolymers of varying PEG side-chain length and grafting ratios were prepared. Detailed preparation procedures and analytical information of the product obtained via this method have been reported elsewhere (1, 2). In this study, three series of polymers synthesized using different PEG molecular weights were employed. The synthesis approach produced a series of polymers of the general composition PLL(20)-*g*-PEG(2), PLL(20)-*g*-PEG(5), and PLL(20)-*g*-PEG(10), with each series consisting of three or four polymer samples differing only in their grafting ratio.

2.2. Preparation of PLL-*g*-PEG-Coated Metal Oxide Substrates. For polymer deposition on oxide substrates, a given PLL(*x*)-*g*[*y*]-PEG(*z*) was dissolved in 10 mM HEPES [Sigma-Aldrich Inc., St. Louis, MO] at a concentration of 1.0 mg/mL. Unless otherwise noted, all HEPES solutions in this study were adjusted to pH 7.4 with 1.0 M NaOH.

Silicon (100) wafers, passivated with silica, were employed as substrates. Prior to immobilization of PLL-*g*-PEG onto the oxide surface, the wafers (0.5 cm × 0.5 cm) were prepared by sonication in toluene (2 min) and in 2-propanol (10 min), extensively rinsed with ultrapure water (EM SCIENCE, Gibbstown, NJ), dried under a gaseous nitrogen flow, and exposed for 2 min to an oxygen plasma (PDC-32G, Harrick Scientific Corp., Ossining, NY). The oxidized substrates were immediately transferred to a 1.0 mg/mL solution of PLL-*g*-PEG in a 10 mM HEPES buffer and incubated there for 40 min. The polymer-coated substrates were then stored in a HEPES solution (in the absence of PLL-*g*-PEG) until use in AFM experiments. Prior to AFM measurements, the polymer-coated substrates were withdrawn from solution, rinsed with a HEPES buffer and ultrapure water to remove free PLL-*g*-PEG, and then dried under a nitrogen flow.

2.3. Friction Measurements with AFM. AFM was used to probe friction forces at the interfaces of polymer-modified substrates under physiological pH solutions. The microscope was equipped with a liquid cell/tip holder (Digital Instruments, Santa Barbara, CA) and controlled by AFM100/SPM 1000 electronics and software (RHK Technology, Inc., Troy, MI). The microscope makes use of a single-tube scanner, on which substrates are rastered with respect to a fixed tip position, and a beam deflection technique, in which light from a laser diode is reflected from the back of a microfabricated cantilever onto a four-quadrant photodetector. Greater details of this instrumental design have been reported previously (10, 11).

Deflection of the cantilever normal to the surface served to monitor surface topograghy and interfacial adhesion. Torsion or twisting of the cantilever was indicative of frictional forces at the tip−sample interface. Kinetic friction data were acquired by monitoring the lateral deflection of the cantilever as a function of the position across the sample surface and applied normal load. This was accomplished by rastering the sample in a line-scan mode while first increasing and then decreasing the applied load. During this procedure, friction and normal forces were measured simultaneously with a scan speed of 1400 nm/s over a distance of 100 nm. Normal loads were determined from the cantilever's nominal spring constant ($k = 0.58$ N/m, manufacturer's reported value) and direct measurements of sample displacement. Friction forces were calibrated through an improved wedge calibration method (12, 13).

AFM measurements were carried out in aqueous HEPES solutions; the composition of the liquid environment encompassing the tip−sample interface was controlled by the transfer of aliquots of solution in and out of the liquid cell through the use of two 5 mL syringes. Sodium borosilicate microspheres (Novascan Technologies, Inc., Ames, IA) with 5.1 μm diameter

affixed to the end of cantilevers were employed as bare sliding counterfaces against the polymer-coated silicon substrates. These colloidal probes were rinsed with dilute HCl (pH 1) and exposed to oxygen plasma for 15 s between measurements to remove any adhering polymer. Normal loads were limited in order to avoid wear of both the probe and polymer-coated surface. A valid comparison of the friction data was enabled by employing the same tip−cantilever assembly throughout a series of friction measurements, while systematically varying other parameters such as the PEG chain length, grafting ratio, or deposition time. Reported friction data represent the average of at least six results obtained at different locations across the surface. Generally, the measurement of at least one tip−sample condition was repeated at the end of a series to ensure that significant wear had not occurred during the course of measurements.

2.4. OWLS. OWLS was carried out on a BIOS-I instrument (ASI AG, Zürich, Switzerland) using a Kalrez (Dupont, Wilmington, DE) flow-through cell with a volume of 16 μL. The waveguide chips (MicroVacuum Ltd., Budapest, Hungary) consisted of a 1-mm-thick glass substrate and a 200-nm-thick $Si_{0.75}Ti_{0.25}O_2$ waveguiding layer at the surface. A silica layer (ca. 12 nm) was sputter-coated on top of the waveguiding layer in a Leybold direct-current magnetron Z600 sputtering unit. Coating conditions and the principles of OWLS investigations have been described in detail elsewhere (14−16). It is important to note that the surface-adsorbed areal mass density determined by OWLS is regarded as a "dry" areal mass density because of the fact that solvent molecules coupled to the adsorbate will not contribute to a change in the refractive index and, thus, do not contribute to the detected adsorbate mass. The reported "dry" areal mass density (m_{dry}) represents the average of three individual experiments. Because this technique is highly sensitive (detection limit $\approx$ 1 ng/cm^2) and allows for the direct online monitoring of macromolecular adsorption (16), a measurement error of less than 1% is expected.

2.5. QCM with Dissipation (QCM-D). All QCM-D measurements were performed with a commercial QCM with dissipation monitoring (Q-Sense, Gothenburg, Sweden) equipped with a home-built laminar flow cell, with a glass window allowing visual monitoring of injection and the exchange of liquids (17). All experiments employed 5 MHz AT-cut quartz sensor crystals, sputter-coated with SiO_2 (also Q-Sense). Details of this setup and measurements have been reported elsewhere (18, 19).

The QCM-D response to mass uptake on the crystal oscillator is reflected in the changes in both the resonant frequency (Δf) and dissipation factor (ΔD) at different overtones. In contrast to OWLS, the QCM-D approach is sensitive to viscoelastic properties and the density of *any* mass coupled to the mechanical oscillation of the quartz crystal. In this case, the adsorbed mass consists of the PLL-*g*-PEG copolymer along with solvent molecules associated with it. A Voigt-based model was therefore used in the analysis (software: *Q-tools*, version 2.0.1), where the adsorbed layer was represented as a homogeneous, viscoelastic film characterized by shear viscosity (η_{shear}), shear modulus (E_{shear}), and film thickness (h_{film}) (20−22).

3. RESULTS

3.1. Influence of the Duration of Polymer Deposition. Using the same microsphere−cantilever assembly throughout, the frictional properties of several PLL(20)-*g*[3.5]-PEG(2)-coated SiO_2 substrates were evaluated as a function of the polymer deposition times: 0.5, 1, 5, 10, 30, and 60 min. The data of Figure 2 portray the distinct influence of the duration of the polymer deposition on interfacial friction, indicating that longer deposition times result in lower friction. This is reflected in the rapid reduction

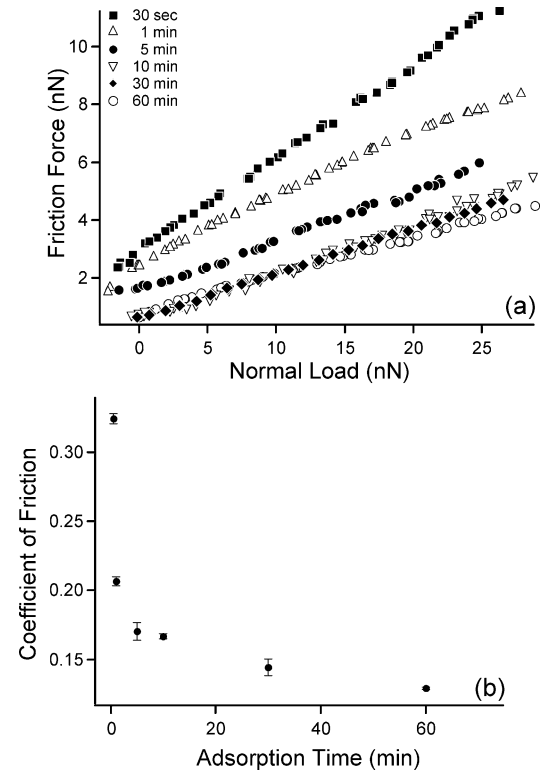

FIGURE 2. (a) Friction versus decreasing load plots of a bare sodium borosilicate microsphere against PLL(20)-*g*[3.5]-PEG(2)-coated SiO_2 substrates prepared at different polymer deposition times. (b) Plot of the coefficient of friction (i.e., slope of the friction−load plots) as a function of the duration of polymer deposition.

in the coefficient of friction (Figure 2b), which is defined as the slope of the friction−load plot (Figure 2a). Within the first 5 min of deposition, the value of the coefficient of friction is reduced to 90% of that measured for the interface of a bare microsphere against a bare oxidized silicon substrate. This reduction in the coefficient of friction was observed to reach a steady-state value after 1 h. The reduction in friction occurring more slowly over the latter portion of this period likely entails the reorganization of the polymer brush at the substrate−solution interface. This behavior was generally observed for all polymer architectures explored in this study.

3.2. Influence of the Polymer Architecture. Interfacial friction was measured for the contact of a 5.1 μm bare borosilicate probe sliding against silicon oxide substrates coated with a series of PLL-*g*-PEG polymer brushes of different PEG molecular weights and lysine/PEG grafting ratios (Figure 3). Three general effects of the polymer architecture on interfacial friction were apparent. First, lower interfacial friction was observed for tribosystems with increased PEG molecular weight (side-chain length), as is exhibited through the maximum friction forces measured at a given normal load. For example, at 30 nN, friction forces decrease with respect to the PEG molecular weight (for a given approximate grafting ratio) in the order of ~10 nN for PLL(20)-*g*(5.7)-PEG(2), ~8 nN PLL(20)-*g*(5.2)-PEG(5), and ~6 nN PLL(20)-*g*(5.8)-PEG(10), in good agreement with prior reports for this polymer brush system (7).

Second, for each PLL-*g*-PEG series, the interfacial friction decreases with decreasing lysine/PEG grafting ratio, as

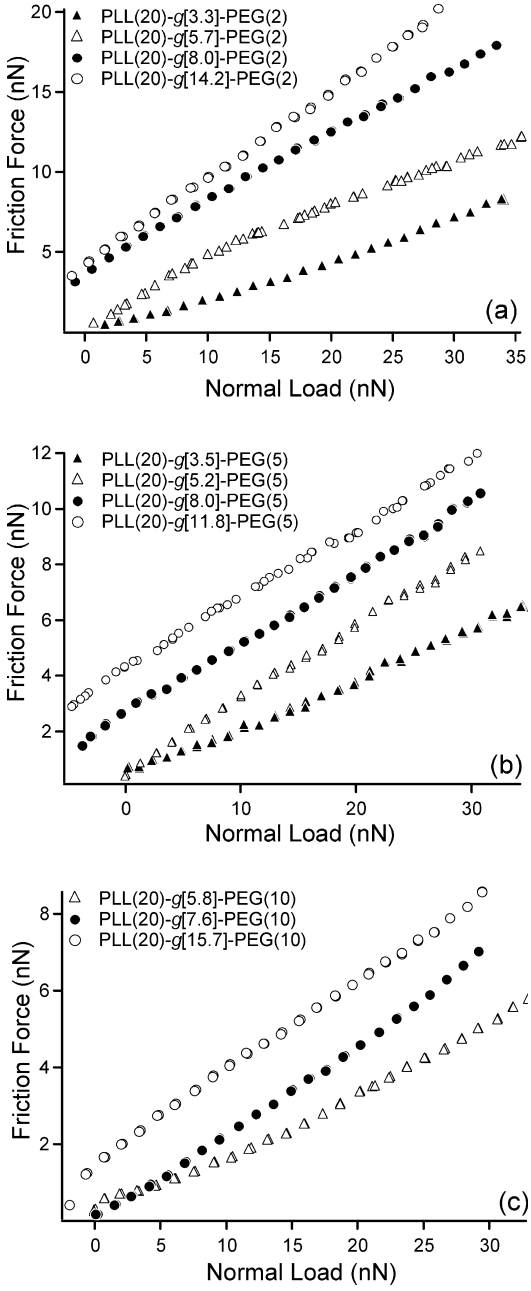

FIGURE 3. Friction versus decreasing load plots for three series of PLL-*g*-PEG polymers: (a) PLL(20)-*g*-PEG(2); (b) PLL(20)-*g*-PEG(5); (c) PLL(20)-*g*-PEG(10). In each series, the polymers vary only in their lysine/PEG grafting ratios. All measurements have been performed using the same AFM microsphere−cantilever assembly for the asymmetrically coated (i.e., bare microsphere/coated substrate) tribointerface. Negative normal loads correspond to adhesive forces existing between the polymer brush and the sodium borosilicate microsphere.

evidenced through both a reduction in the *magnitude* of the friction forces at a specific load and in the coefficient of friction (*slope* of the friction−load plot). For each series, the lowest coefficients of friction are observed for the lowest grafting ratio, corresponding to the greatest density of PEG chains grafted to the PLL backbone.

Third, interfacial adhesion between the bare sodium borosilicate microsphere and the adsorbed polymer film is reduced/eliminated at respectively lower grafting ratios for the systems composed of higher molecular weight PEG. For nonadhesive contacts, the friction force is expected to be zero at zero normal load; adhesion increases the effective contact area between the probe and substrate as a function of the normal load and results in finite contact areas, and corresponding finite friction forces, at zero and negative normal loads. In the PLL-*g*-PEG system, the friction−load plots approach the nonadhesive limit as the number and size of PEG chains increases. Where adhesive forces are detected in the case of high grafting ratios, the interaction likely entails partially exposed charges on the PLL backbone and surface charges on the bare oxide probe tip.

Table 1 summarizes the data for the coefficient of friction (μ) versus the PEG molecular weight (z) and lysine/PEG grafting ratio (y). Additionally, data characterizing the adsorption of PLL-*g*-PEG from an aqueous solution composed of the physiological buffer, HEPES (a good solvent), is included in terms of the "dry" polymer mass (m_{dry}) and "wet" polymer mass measured with OWLS and QCM-D, respectively. From m_{dry} and the parameters of the polymer architecture (x, y, and z), the PEG surface packing density (σ), or the number of PEG chains per unit area of substrate, may be calculated. An effective solvated film thickness (h_{film}) can also be estimated from this areal PEG density and the "wet" mass of the solvated polymer. In each case, the reported values of the effective film thickness systematically scale with the polymer architecture, increasing for greater PEG chain lengths (z) and decreasing for higher grafting ratios (y).

4. DISCUSSION

4.1. Influence of the Duration of Polymer Deposition. The kinetics and thermodynamics of polyelectrolyte adsorption on oxide surfaces have been extensively studied (23, 24). In general, polyelectrolytes will adsorb spontaneously in order to neutralize charges on the surface. The initial rate of adsorption is diffusion-limited and, therefore, a function of the degree of swelling (size) of the polyelectrolyte in the bulk solution (23). Low ionic strengths preclude the screening of electrostatic interactions, thus causing the polyelectrolytes to adsorb irreversibly. Moreover, once on the surface, spreading and reconformation is slow, resulting in dangling loops and tails as well as conformational heterogeneity and overcompensation of surface charge (24). The adsorption of comb copolymers, in particular, has been studied using self-consistent-field methods (25). For comb copolymers with an "adsorbing backbone" (e.g., a polyelectrolyte) and "nonadsorbing teeth", the teeth will tend to protrude into the solution to compensate for the decrease in entropy, resulting in confinement and thus decreasing the critical adsorption energy. Moreover, the volume fraction profiles of adsorbed comb copolymers with narrow spacing between teeth are expected to exhibit brushlike behavior.

The adsorption performance of PLL-based polymers has also been studied, with PLL-*g*-PEG found to adsorb spontaneously from aqueous solution onto many oxide surfaces (1, 2). Electrostatic interaction between cations on the PLL backbone and the negative charge on the oxide surface lead to strong attraction under appropriate solution conditions.

Table 1. Summary of Data for the Three PEG Chain Length Series of PLL(*x*)-*g*[*y*]-PEG(*z*), Varying Only in Lysine/PEG Grafting Ratios (*y*)[a]

polymer architecture PLL(*x*)-*g*[*y*]-PEG(*z*)	*y* (lysine/PEG)	m_{dry}, ng/cm^2	σ, nm^{-2}	h_{film}, nm	μ
PLL(20)-*g*-PEG(2)	3.3	75.183	0.18	5.91	0.20 ± 0.04
	5.7	55.45	0.12	5.01	0.431 ± 0.005
	8.0	45.06	0.09	4.19	0.75 ± 0.03
	14.2	36.76	0.05	3.09	0.88 ± 0.04
PLL(20)-*g*-PEG(5)	3.5	147.57	0.16	11.18	0.199 ± 0.006
	5.2	111.95	0.12	9.75	0.308 ± 0.006
	8.0	88.27	0.09	9.35	0.46 ± 0.02
	11.8	59.81	0.05	6.98	0.58 ± 0.03
PLL(20)-*g*-PEG(10)	5.8	133.76	0.07	15.6	0.162 ± 0.003
	7.6	109.14	0.06	12.9	0.226 ± 0.001
	15.7	55.76	0.03	10.01	0.35 ± 0.01

[a] *x* and *z* are PLL and PEG molecular weights in kDa, respectively. Note: m_{dry}, "dry" mass measured by OWLS; h_{film}, thickness of the "wet" brush determined from QCM-D measurements; σ, calculated PEG surface packing density; μ, coefficient of friction.

In general, the pH of the medium must be above the isoelectric point (IEP) of the oxide, where it will be negatively charged, and below the pK_a of the primary amines on PLL, where it will be positively charged (1). In the present study, the adsorption of PLL(20)-*g*[3.5]-PEG(2) onto SiO_2-passivated surfaces has been performed from 1.0 mg/mL polymer solutions in 10 mM HEPES, adjusted to the physiological pH (7.4). Because the IEP of SiO_2 is ∼2.0 (26, 27), its surfaces are negatively charged under these conditions, while the amino groups (p$K_a \approx 10$) would be positively charged.

The kinetics of adsorption of PLL-*g*-PEG has been previously reported from OWLS measurements for various oxide surfaces, including Nb_2O_5, $Si_{0.4}Ti_{0.6}O_2$, and TiO_2 (1, 2). It has been observed that adsorption takes place rapidly and irreversibly, with 95% of the final adsorbed mass reached within the first 5 min, followed by a stable plateau after 20 min. The plot of the coefficient of friction versus deposition time in Figure 2 essentially tracks the OWLS kinetic plot, with 90% of the reduction in friction occurring within the first 5 min, followed by a slow leveling off after 30 min. These friction measurements were performed using the same tip−cantilever assembly on several samples prepared at different deposition times, in contrast to the OWLS measurements, which were performed continuously over time.

The presence of a solvated polymer layer, especially the outer layer composed of water-soluble, flexible PEG side chains, proves to be favorable to the reduction in friction. The observed lubricity with the duration of polymer deposition is, therefore, a function of the development of this solvated polymer layer on the surface. Not only is the coverage increased over time, but as discussed below, the increase in the packing density drives the PEG chains to form more extended conformations as well.

4.2. Influence of the Polymer Architecture. The time dependence of the friction reduction with PLL-*g*-PEG adsorption suggests that the frictional properties of these interfaces are closely related to the areal density of the PEG chains immobilized near the surface. The full effect of this areal density is revealed through an analysis of the coupled contribution of the PEG chain length and grafting ratio to the interfacial friction. To determine the number density of PEG chains on the surface, it is assumed that the PLL backbone lies nearly flat on the surface and that the PEG chains are protruding into the solution in a brushlike fashion, as predicted for comb copolymers with "adsorbing backbones" and "nonadsorbing teeth". Table 2 presents the data for the "wet" thickness of the polymer film (from Table 1), comparing it with the theoretical thickness (h_0) predicted from brush scaling laws: $h_0 = aN\sigma^{1/3}$, where *a* relates to the monomer length, *N* the number of monomer units, and σ the PEG packing density (28, 29).

Table 2. "Wet" Brush Thickness Measured by QCM-D (h_{film}) Compared with the Brush Thickness Calculated from Scaling Laws ($h_0 = aN\sigma^{1/3}$)

polymer architecture PLL(*x*)-*g*[*y*]-PEG(*z*)	*y* (lysine/PEG)	h_{film}, nm	h_0, nm
PLL(20)-*g*-PEG(2)	3.3	5.91	4.66
	5.7	5.01	4.03
	8.0	4.19	3.63
	14.2	3.09	3.12
PLL(20)-*g*-PEG(5)	3.5	11.18	11.18
	5.2	9.75	10.05
	8.0	9.35	9.08
	11.8	6.98	7.75
PLL(20)-*g*-PEG(10)	5.8	15.6	17.27
	7.6	12.9	16.01
	15.7	10.01	12.38

In bulk solution, the radius of gyration (R_g) reflects the conformation of a linear polymer that follows the statistics of a self-avoiding random walk; this is considered to be its unperturbed dimension. Upon confinement to a surface, adsorbed polymers can be described in the form of a two-dimensional lattice with an average distance between graft points (*L*), which scales with the packing density, as shown below. If *L* is larger than R_g, the polymer molecules maintain their unperturbed dimension on the surface. However, when *L* becomes smaller than R_g, adjacent polymer chains begin to overlap and assume more stretched conformations due to repulsive (excluded volume) interactions (28−30). The ratio $L/2R_g$ can be used as a gauge for the extent of stretching of a polymer grafted onto a surface (1, 31, 32); it

includes information about both the polymer's *dimensions* and *packing density*. For the series of PLL-*g*-PEG polymers, the polymer dimension would be that of the PEG side chains ($R_g \propto z$) that are expected to protrude perpendicular to the surface, while the polymer packing density will be closely related to the grafting ratio ($\sigma \propto y^{-1}$).

Estimates of the radius of gyration can be made using an empirical equation derived from static light scattering experiments (31, 33),

$$R_g = 0.181N^{0.58}\ (\text{nm}) \qquad (1)$$

where N is the degree of polymerization. From this equation, the unperturbed dimensions of the PEG side chains of different molecular weights are estimated to be 1.65 nm for 2 kDa PEG, 2.82 nm for 5 kDa PEG, and 4.21 nm for 10 kDa PEG. The prefactor in the above equation relates to the PEG's monomer unit length. In turn, the average grafting distance can be estimated from the surface packing density, assuming a hexagonal close-packed lattice arrangement (31, 32).

$$L = \left(\frac{4}{3}\right)^{1/4}\sigma^{-1/2} \approx \sigma^{-1/2} \qquad (2)$$

Table 1 presents values for σ that are equivalent to the number of PEG chains per unit area (nm^{-2}), as calculated from the "dry" mass (from OWLS) of PLL-*g*-PEG adsorbed on the surface and the parameters (x, y, and z) of the polymer architecture. As such, L relates to both the lysine/PEG grafting ratio and how the PLL-*g*-PEG copolymer stacks side-by-side on the surface during adsorption.

On the basis of these values, the coefficient of friction, determined from data in Figure 3 and presented in Table 1, can be plotted as a function of $L/2R_g$, a parameter that expresses the relative degree of extension of the PEG brush on the surface in terms of its chain length and packing density.

$L/2R_g$ values below 1 represent the regime where lateral interaction between PEG chains begins to occur and the polymer begins to stretch relative to its unperturbed dimensions. As architectures are modified such that $L/2R_g$ values approach 0.5, scaling theory predicts that strong stretching occurs and the adsorbed polymer switches from the mushroom to the brush regime (28−30). The data of Figure 4 portray a reduction in friction with decreasing values of $L/2R_g$, with the lowest friction observed at $L/2R_g \approx 0.5$, supporting the idea that the conformational state of the PEG chains contributes to the lubricity of the PLL-*g*-PEG copolymer system. At higher grafting ratios, changes in the adhesive component of friction also contribute to the observed trend; however, the conformational state represents the primary influence because the trend is clearly propagated to lower grafting ratios.

This observation is underscored by the extent of the data derived from a matrix of architectures varying in both the PEG molecular weight and grafting density. The coefficient of friction values of PLL-*g*-PEG polymers with 2 kDa PEG side

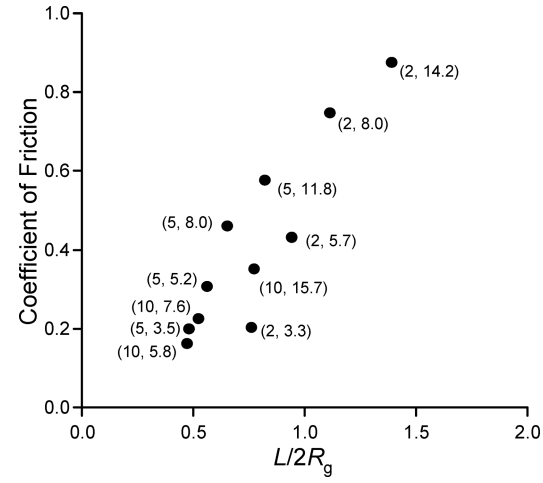

FIGURE 4. Plot of the coefficient of friction versus $L/2R_g$, estimated from eqs 1 and 2. The data labels (z, y) indicate the PEG molecular weight in kDa (z) and the lysine/PEG grafting ratio (y).

chains are observed to lay slightly outside the predicted relationship between friction and strong stretching. This result can be rationalized through the potential for a closer proximity of the PLL backbone with shorter side chains to the surface, thus producing a greater effective surface packing density and leading to an overestimation of L in these cases. In general, it is seen that brush architectures possessing longer PEG side chains and lower grafting ratios (relatively more PEG chains attached to the PLL backbone) exhibit the lowest frictional forces.

It is also noteworthy to observe that the tribological behavior of the PLL-*g*-PEG system, namely, the lowest friction corresponding to $L/2R_g \approx 0.5$, exhibits a trend remarkably similar to that observed for the resistance to protein adsorption for PLL-*g*-PEG-coated surfaces (1, 31). In general, reductions in the surface energy and increases in steric repulsion are known to enhance protein resistance; in addition, the amount of bound water at the interacting interface has also been considered in the context of PLL-*g*-PEG-coated surfaces. Similarly here, the reductions in friction observed for the series of thin polymer films, essentially equivalent in chemical composition at the sliding interface, suggest an important role of the solvent molecules. It is surmised that the conformational changes of the polymer associated with an extended or brushlike state in which water is effectively complexed also produce low shear strength at the sliding interface.

Finally, it is important to note that the results and discussion presented here correspond to tribological properties of adsorbed bottle brush systems, measured on a microscopic scale under boundary conditions in the absence of interfacial wear. In macroscopic tribological settings in which the polymer is removed at the sliding interface through shearing action, a more complex relationship between friction and molecular architecture is anticipated because of the contribution of interfacial binding and adsorption kinetics. Additional differences in the relationship between friction and structure are also likely for surfaces at which PEG moieties have been directly attached.

5. CONCLUSION

Frictional properties of PLL-*g*-PEG-coated silicon oxide surfaces have been systematically studied by AFM, as a function of the deposition time and polymer architecture, employing a 5.1-μm-diameter sodium borosilicate probe under aqueous media at physiological pH. The most significant reduction in friction occurred within the first 5 min of substrate exposure to the polymer solution, after which a more moderate reduction was observed owing to the conformational reorganization of the polymer film. Friction between the polymer-coated substrate and colloidal probe was observed to systematically vary with the polymer architecture, specifically, the PEG chain length and the lysine/PEG grafting ratio. The coefficient of friction decreased with respect to increased PEG molecular weight and decreased lysine/PEG ratio. The general friction response of PLL-*g*-PEG as a function of the polymer architecture has been rationalized in terms of the spatial density of the PEG side chains. This areal density has been characterized in terms of the distance between PEG chains on the surface (L), related to the grafting ratio and coverage, and the radius of gyration (R_g) of the side chains, related to the PEG molecular weight. It was observed that the lowest friction was encountered at $L/2R_g \approx 0.5$, the point where brush scaling theory predicts the onset of strong stretching. This trend is analogous to the increase in protein resistance previously observed (1, 31) for PLL-*g*-PEG-coated surfaces within the same strong stretching regime. The observed trends in frictional properties for the matrix of polymer brush architectures are highly relevant to the design of future applications entailing brush structures as boundary layer lubricants or as biomimetic lubricants (34). Specifically the results highlight the need for tailoring the local conformation of brush side chains while simultaneously maintaining the backbone functionality required for adsorption at interfaces.

Acknowledgment. This work has been supported by the U.S. Air Force Office of Scientific Research under Contract F49620-02-1-0346. The authors are also grateful for financial support received from the TopNano21 Program of the Council of the Swiss Federal Institutes of Technology (ETH-Rat).

REFERENCES AND NOTES

(1) Kenausis, G. L.; Vörös, J.; Elbert, D. L.; Huang, N.; Hofer, R.; Ruiz-Taylor, L.; Textor, M.; Hubbell, J. A.; Spencer, N. D. *J. Phys. Chem. B* **2000**, *104*, 3298.
(2) Huang, N.; Michel, R.; Voros, J.; Textor, M.; Hofer, R.; Rossi, A.; Elbert, D. L.; Hubbell, J. A.; Spencer, N. D. *Langmuir* **2001**, *17*, 489.
(3) Elbert, D. L.; Hubell, J. A. *Chem. Biol.* **1998**, *5*, 177.
(4) Ruiz-Taylor, L. A.; Martin, T. L.; Wagner, P. *Langmuir* **2001**, *17*, 7313.
(5) Huang, N.; Vörös, J.; De Paul, S. M.; Textor, M.; Spencer, N. D. *Langmuir* **2002**, *18*, 220.
(6) Spencer, N. D.; Perry, S. S.; Lee, S.; Müller, M.; Pasche, S.; De Paul, S. M.; Textor, M.; Yan, X.; Lim, M. S. In *Tribological Research and Design for Engineering Systems: Proceedings of the 29th Leeds-Lyon Symposium (Tribology and Interface Engineering)*; Dowson, D., Lubrecht, A. A., Dalmaz, D., Priest, M., Eds.; Elsevier Science: New York, 2003; pp 411−416.
(7) Yan, X.; Perry, S. S.; Spencer, N. D.; Pasche, S.; De Paul, S. M.; Textor, M.; Lim, M. S. *Langmuir* **2004**, *20*, 423.
(8) Lee, S.; Müller, M.; Ratoi-Salagean, M.; Vörös, J.; Pasche, S.; De Paul, S. D.; Spikes, H. A.; Textor, M.; Spencer, N. D. *Tribol. Lett.* **2003**, *15*, 231.
(9) Müller, M.; Lee, S.; Spikes, H. A.; Spencer, N. D. *Tribol. Lett.* **2003**, *15*, 395.
(10) Perry, S. S. *MRS Bull.* **2004**, *29*, 478.
(11) Perry, S. S.; Somorjai, G. A.; Mate, C. M.; White, R. L. *Tribol. Lett.* **1995**, *1*, 233.
(12) Ogletree, D. F.; Carpick, R. W.; Salmeron, M. *Rev. Sci. Instrum.* **1996**, *67*, 3298.
(13) Varenberg, M.; Etsion, I.; Halperin, G. *Rev. Sci. Instrum.* **2003**, *74*, 3362.
(14) Kurrat, R.; Textor, M.; Ramsden, J. J.; Böni, P.; Spencer, N. D. *Rev. Sci. Instrum.* **1997**, *68*, 2172.
(15) Vörös, J.; Ramsden, J. J.; Csúcs, G.; Szendrö, I.; De Paul, S. M.; Textor, M.; Spencer, N. D. *Biomaterials* **2002**, *23*, 3699.
(16) Vörös, J. *Biophys. J.* **2004**, *87*, 553.
(17) Rodahl, M.; Höök, F.; Krozer, A.; Brzezinski, P.; Kasemo, B. *Rev. Sci. Instrum.* **1995**, *66*, 3924.
(18) Müller, M. T.; Yan, X.; Lee, S.; Perry, S. S.; Spencer, N. D. *Macromolecules* **2005**, *38*, 3861.
(19) Müller, M. T.; Yan, X.; Lee, S.; Perry, S. S.; Spencer, N. D. *Macromolecules* **2005**, *38*, 5706.
(20) Voinova, M. V.; Rodahl, M.; Jonson, M.; Kasemo, B. *Phys. Scr.* **1999**, *59*, 391.
(21) Bandey, H. L.; Hillman, A. R.; Brown, M. J.; Martin, S. J. *Faraday Discuss.* **1997**, *107*, 105.
(22) Larsson, C.; Rodahl, M.; Höök, F. *Anal. Chem.* **2003**, *75*, 5080.
(23) Hoogeveen, N. G.; Stuart, M. A. C.; Fleer, G. J. *J. Colloid Interface Sci.* **1996**, *182*, 133.
(24) Hoogeveen, N. G.; Stuart, M. A. C.; Fleer, G. J. *J. Colloid Interface Sci.* **1996**, *182*, 146.
(25) van der Linden, C. C.; Leermakers, F. A. M.; Fleer, G. J. *Macromolecules* **1996**, *29*, 1000.
(26) Lin, X.; Creuzet, F.; Arribart, H. *J. Phys. Chem.* **1993**, *97*, 7272.
(27) Parks, G. A. *Chem. Rev.* **1965**, *65*, 177.
(28) de Gennes, P. G. *Macromolecules* **1980**, *13*, 1069.
(29) de Gennes, P. G. *Adv. Colloid Interface Sci.* **1987**, *27*, 189.
(30) Hansen, P. L.; Cohen, J. A.; Podgornik, R.; Parsegian, V. A. *Biophys. J.* **2003**, *84*, 350.
(31) Pache, S.; De Paul, S. M.; Vörös, J.; Spencer, H. D.; Textor, M. *Langmuir* **2003**, *19*, 9216.
(32) Henn, G.; Bucknall, D. G.; Stamm, M.; Vanhoorne, P.; Jérôme, R. *Macromolecules* **1996**, *29*, 4305.
(33) Kawaguchi, S.; Imai, G.; Suzuki, J.; Miyahara, A.; Kitano, T.; Ito, K. *Polymer* **1997**, *38*, 2885.
(34) Lee, S.; Spencer, N. D. *Science* **2008**, *319*, 575.

AM900101M